The Journal of Chemical Physics

Electron affinity of tantalum and excited states of its anion

Cite as: J. Chem. Phys. **157**, 044302 (2022); https://doi.org/10.1063/5.0101903
Submitted: 04 June 2022 • Accepted: 06 July 2022 • Accepted Manuscript Online: 06 July 2022 • Published Online: 01 August 2022

Sheng Li, Xiaoxi Fu, Xiaolin Chen, et al.

The Journal of Chemical Physics ARTICLE scitation.org/journal/jcp

Electron affinity of tantalum and excited states of its anion

Cite as: J. Chem. Phys. 157, 044302 (2022); doi: 10.1063/5.0101903
Submitted: 4 June 2022 • Accepted: 6 July 2022 •
Published Online: 1 August 2022

Sheng Li,[1] Xiaoxi Fu,[1] Xiaolin Chen,[1] Yuzhu Lu,[1] and Chuangang Ning[1,2,a)]

AFFILIATIONS

[1] Department of Physics, State Key Laboratory of Low Dimensional Quantum Physics, Tsinghua University, Beijing 100084, China

[2] Collaborative Innovation Center of Quantum Matter, Beijing 100084, China

[a)] **Author to whom correspondence should be addressed:** ningcg@tsinghua.edu.cn

ABSTRACT

The tantalum anion has the most complicated photoelectron spectrum among all atomic anions of transition elements, which was the main obstacle to accurately measure its electron affinity via the generic method. The latest experimental value of the electron affinity of Ta was 0.323(12) eV, reported by Feigerle *et al.* [J. Chem. Phys. **74**, 1580 (1981)]. In the present work, we report the high-resolution photoelectron spectroscopy of Ta^- via the slow-electron velocity-map imaging method combined with a cryogenic ion trap. The electron affinity of Ta was measured to be 2652.38(17) cm^{-1} or 0.328 859(23) eV. Three excited states $^5D_1$, $^3P_0$, and $^5D_2$ of Ta^- were observed, and their energy levels were determined to be 1169.64(17) cm^{-1} for $^5D_1$, 1735.9(10) cm^{-1} for $^3P_0$, and 2320.1(20) cm^{-1} for $^5D_2$ above the ground state $^5D_0$, respectively.

I. INTRODUCTION

Most elements can form stable anions. The extra electron is weakly bound via the polarization and correlation effects. The short-range potential tends to support only one bound state, and atomic anions may have a few fine-structure splittings. As a sharp contrast, the long-range Coulomb potential of neutral atoms and positive ions can have infinite bound states. However, strong electron correlation effects do allow the existence of a few bound excited states of a few atomic anions. For example, Os^-,[1–5] La^-,[5–11] Ce^-,[12–14] Th^-,[15–17] and U^-[18] have been experimentally confirmed to have bound states with opposite parities, which makes them potential candidates for laser cooling of negative ions since a fast electric dipole cycling transition is needed. Electron Affinity (EA) is an important parameter that measures the ability of an atom to obtain an electron to form a negative ion. It is widely involved in plasma physics and atmospheric chemistry. Tantalum is an element in group VB. The latest experimental value of EA(Ta) was 0.323(12) eV, reported by Feigerle *et al.* in 1981.[19] For elements V and Nb in the same group, we accurately measured their electron affinity and fine structures by using our first-generation spectrometer and obtained EA(V) = 0.527 66(20) eV[20] and EA(Nb) = 0.917 40(6) eV.[21] The high accuracy was obtained via the slow-electron velocity-map imaging (SEVI) method.[22–25] SEVI has a very high-energy resolution, typically a few cm^{-1} near the photodetachment threshold.[26] This is an essential ability for resolving the dense electronic states. When we tried the experiment for Ta^-, the very complicated photoelectron spectrum of Ta^- and the interference from its hydride anion TaH^- hindered our further accurate measurement. The difficulty we faced was similar to the situation encountered by Feigerle *et al.* in 1981.[19] Actually, they concluded that Ta^- had the most complicated photoelectron spectrum among all atomic anions. The ion intensity of TaH^- generated by our laser ablation ion source was an order of magnitude stronger than that of Ta^-. The temperature of TaH^- ions generated with this method was very high, ~1000 K. The photoelectron spectrum of hot TaH^- ions had a very broad distribution due to thermal broadening. Our preliminary experiment showed that the weak signal of Ta^- was nearly buried in the noisy background contaminated by TaH^-. The poor signal-to-noise ratio impeded the further accurate measurement of EA(Ta). Other early transition metals have a similar problem. Signals of their hydride anions are always dominant in the laser ablation ion source. To overcome this obstacle, we built a second-generation apparatus recently, which combined a SEVI method and a cryogenic ion trap. The cold ion trap can effectively cool the temperature of molecular anions down to ~10 K via buffer-gas cooling. As a result, the

photoelectron spectra of molecular anions become very sharp and clean. Moreover, the cold ion trap can effectively reduce the trapped ion packets' size and thermal energy, significantly improving the mass resolution ($m/\Delta m$). The cold ion trap and the high-resolution mass spectrometer can substantially reduce the interference of hydride anions. With the new apparatus, we have successfully measured the EA values of Hf,[27] Ti,[25] and partial elements of lanthanides and actinides.[9,16–18,28,29] In the present work, we report the accurate measurement of the EA value of Ta using our second-generation apparatus.

Research on the electron affinity of Ta can date back to 1968 when Zollweg predicted EA(Ta) = 0.15 eV through a semiempirical extrapolation.[30] Scheer *et al.* measured the sublimation rate of the metal at a fixed temperature in 1969 and obtained EA(Ta) = 0.8(3) eV.[31] In 1982, Cole and Perdew used a self-interaction corrected scheme on the local spin-density approximation to predict EA(Ta) = 1.0 eV.[32] In 2009, Figgen and co-workers calculated electron affinities of the 5d transition metals using the high-level coupled-cluster method with an energy-consistent pseudopotential and obtained EA(Ta) = 0.31 eV.[33]

The photoelectron spectroscopy of Ta^- reported by Feigerle in 1981 was the only spectroscopic investigation of the electronic structure of Ta^- to the best of our knowledge.[19] They observed a very complicated photoelectron spectrum with a photodetachment laser at 488 nm interacting with the ion beam of Ta^-. Their spectrum included 15 peaks assigned to 23 transition channels from four different states of negative ions. Despite TaH^- impurity having been subtracted, two regions of the spectrum (for electron kinetic energies in ranges around 0.3–0.8 and 1.2–1.4 eV using the 488 nm photodetachment laser) still had the contamination of hydride anions. They assigned the ground state of Ta^- as $5d^36s^2\ ^5D_0$ and obtained EA(Ta) = 0.323(12) eV. Three excited states $^5D_1$, $^5D_2$, and $^3P_0$ of Ta^- were also observed. The energy gaps between the states were determined to be $\Delta E(^5D_1 - {}^5D_0)$ = 1070(110) cm^{-1}, $\Delta E(^5D_2 - {}^5D_0)$ = 2240(120) cm^{-1}, and $\Delta E(^3P_0 - {}^5D_0)$ = 1750(110) cm^{-1}.

II. METHODS

The present experiment was conducted on our second-generation photoelectron-imaging spectrometer equipped with a cryogenic ion trap. Details of the spectrometer have been described in our previous work.[25] Briefly, negative ions were generated by focusing a 532 nm Nd:YAG pulsed laser onto a metal disk. The negative ions were then accumulated and confined in an octupole radio-frequency (rf) ion trap. The trapped negative ions lost their kinetic energy through collisions with the buffer gas, which was delivered by a pulsed valve. The ion trap was mounted on a cold head connected to a liquid helium refrigerator with a controllable temperature range of 5–300 K. The typical buffer gas was He or H_2. After sufficient collisions with the buffer gas, the temperature of trapped ions can be cooled down to ~10 K. Our experiences showed that H_2 gas was more effective in quenching the excited states than He. The trapping time can be adjusted in the range of 3–45 ms. The ion trap can be turned off and let ions directly fly through it, so excited states with a short lifetime have more chance to survive for the later photodetachment experiment. This option is beneficial for identifying the excited states since their intensities will change when the trapping time is altered. The trapped ions can be ejected out and were analyzed by a Wiley–McLaren type time-of-flight (TOF) mass spectrometer.[34] The ions of interest were selected and then were perpendicularly crossed by a laser beam in the interaction zone of the velocity-map imaging system. The photoelectrons from the same photodetachment channel of negative ions expanded into a spherical shell and were projected onto a phosphor screen. The fluorescence was recorded via a charge-coupled device (CCD) camera. Typically, 30 000–50 000 laser shots were assembled to form one photoelectron image with a repetition rate of 20 Hz. The photodetachment laser used in the present work was a tunable dye laser with a linewidth of 0.06 cm^{-1}. The photon energy $h\nu$ was further monitored via a HighFinesse WS6-600 wavelength meter with an accuracy of 0.02 cm^{-1}. For negative ions with a complicated electronic structure, it is a nontrivial task to reliably assign the observed spectra since many photodetachment channels are opened at higher photon energy. To resolve the problems, we further extended the tunable range of our dye laser system to the infrared region via a difference frequency generation (DFG) system recently. At lower photon energy, only a few photodetachment channels are opened, and the energy resolution also increases, thanks to the feature of the SEVI method. The infrared laser was produced by a nonlinear DFG effect in a $LiNbO_3$ crystal between a dye laser and a residual 1064 nm laser, which was the fundamental output of the pump laser. The tuning range of our DFG system was 1.5–4.2 μm, and the linewidth of the DFG light was 1 cm^{-1}, limited mainly by the linewidth of the unseeded 1064 nm laser.

The distribution of outgoing photoelectrons has a cylindrical symmetry when a linearly polarized laser is used. Therefore, the recorded 2D projection includes all the information required for reconstructing the 3D photoelectron spherical shell through an inverse Abel transformation or the maximum entropy velocity Legendre reconstruction (MEVELER) method.[35] MEVELER was used in the present work since it has no annoying center-line-artifact problem.[35] The binding energy (BE) of the electron before photodetachment is given by BE = $h\nu - \alpha r^2$. $h\nu$ is the photon energy of the detachment laser, r is the radius of the spherical shell, and α is a calibration coefficient, which can be obtained by changing the photon energy $h\nu$ or by measuring the atomic anion with a well-known electron affinity. The photoelectron angular distribution (PAD) can also be derived from the reconstructed distribution. For one-photon detachment with a linearly polarized laser, the PAD is given by[36–39]

$$I(\theta) = \frac{\sigma}{4\pi}[1 + \beta P_2(\cos\theta)],$$

where θ is the angle of the outgoing electron relative to the laser polarization and $P_2()$ is the second-order Legendre polynomial. σ is the total photodetachment crosssection. β is defined as the asymmetry parameter lying between −1 and 2, which depends on the electronic state and the photon energy.

III. RESULTS AND DISCUSSION

Figure 1 shows the photoelectron energy spectra of Ta^- at photon energies $h\nu$ = 11 603 and 12 759 cm^{-1}. The imaging voltage was −650 V. The spectrum collected with the trap-on mode at

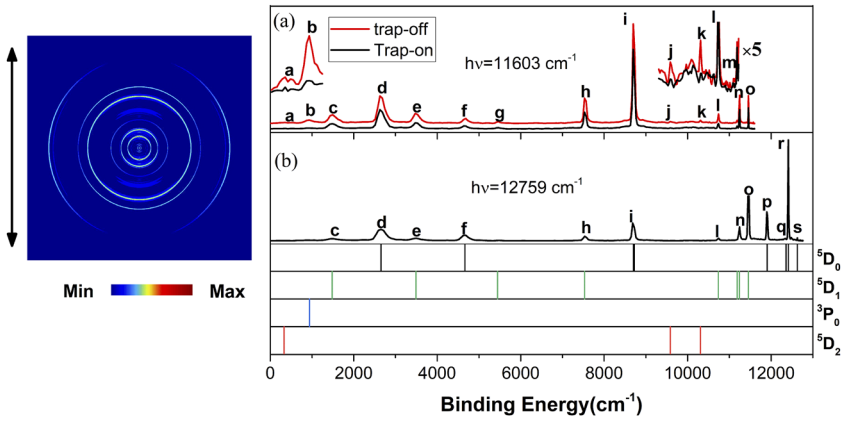

FIG. 1. (a) Photoelectron energy spectra of Ta^- at photon energy $h\nu$ = 11 603 cm^{-1}. The upper line (in red) is for a trap-off mode, while the bottom line (in black) is for a trap-on mode. The weak peaks were blown up by a factor of 5 for a better view. (b) Photoelectron energy spectra of Ta^- at $h\nu$ = 12 759 cm^{-1} with a trap-on mode. The image on the left shows the photoelectron velocity-map image of Ta^- at $h\nu$ = 11 603 cm^{-1} with a trap-on mode. The double-headed arrow represents the polarization direction of the photodetachment laser. The vertical spikes under the spectra indicate the energy levels of the neural atom Ta from different initial states of Ta^- with labels on the right side.

$h\nu$ = 11 603 cm^{-1} was compared with the spectrum with the trap-off mode in Fig. 1(a). With the trap-on mode, the ions were stored in the ion trap for 45 ms at room temperature, so only these states with lifetimes comparable to 45 ms can be observed with this mode. With the trap-off mode, it took about 0.5 ms for Ta^- ions to fly from the ion source to the photodetachment zone. Therefore, the short-lived excited states have more chances to survive with the trap-off mode. Since the energy levels of neutral Ta atoms are well known with high accuracy, the energy gaps among the energy levels can be taken as a fingerprint for the assignment of the observed peaks. The peaks d, f, and i can be unambiguously assigned to the photodetachment transitions from the ground state of Ta^-. The extra peaks a, b, j, and k that appear only at the trap-off mode are related to the excited states of Ta^-. In principle, any peak from the ground state of Ta^- can be used to measure the electron affinity of Ta since the energy levels of the neutral atom Ta are well known. However, the binding energies of peaks d, f, and i are not in the tuning range of our dye laser system. To find a suitable photodetachment channel, we collected a spectrum at higher photon energy $h\nu$ = 12 759 cm^{-1}. The strong peak r, assigned as Ta $5d^46s\ ^6D_{1/2}$ ← Ta^- $5d^46s^2\ ^5D_0$, was also from the ground state of Ta^-, and its binding energy was covered by our dye laser. Therefore, peak r was chosen for the electron affinity measurement. Based on the well-known energy levels of Ta, the work by Feigerle *et al.* in 1981,[19] and the selection rules of photodetachment, all peaks observed in Fig. 1 can be identified, which were indicated by the spikes below the spectra. The term symbol of each initial state of Ta^- was labeled on the right.

The primary measurement of the binding energy of peak r [Ta $5d^46s\ ^6D_{1/2}$ ← Ta^- $5d^46s^2\ ^5D_0$] in Fig. 1 helped narrow down the range for performing a series of low-kinetic-energy photoelectron measurements to achieve high accuracy of the EA value. The photon energy was scanned from 12 440.48–12 520.62 cm^{-1} with a step of 20 cm^{-1}, slightly above the threshold. Since the kinetic energy of photoelectrons is proportional to the squared radius of the circle, the binding energy (BE) of peak r is given by BE = $h\nu - \alpha r^2$. As shown in Fig. 2, BE was obtained through a linear fitting of $h\nu$ vs r^2, and the intercept of the fitted line is the *BE* value. Thus, the binding energy of peak r [Ta $5d^46s\ ^6D_{1/2}$ ← Ta^- $5d^46s^2\ ^5D_0$] was determined to be 12 411.40(0.18) cm^{-1}. The linewidth of the detachment laser (0.06 cm^{-1}) has been included in the uncertainty 0.18 cm^{-1}. The energy level of the final neutral Ta $5d^46s\ ^6D_{1/2}$ state is 9758.97 cm^{-1} above its ground state Ta $5d^36s^2\ ^4F_{3/2}$.[40] Therefore, the preliminary EA value of Ta was determined to be 2652.43(18) or 0.328 859(23) eV by subtracting 9758.97 from 12 411.40(0.18) cm^{-1}. This value is further optimized to be 2652.38(17) or 0.328 859(23) eV since multiple channels from the ground state of Ta^- were observed.

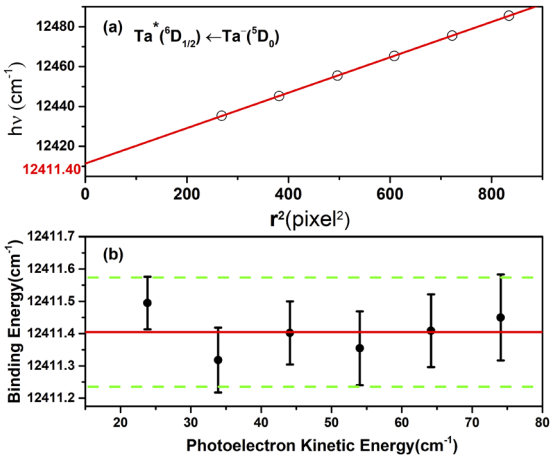

FIG. 2. (a) Photon energy $h\nu$ vs r^2 for transition r (Ta $5d^46s\ ^6D_{1/2}$ ← Ta^- $5d^46s^2\ ^5D_0$). The solid line in red is the linear least-squares fitting. (b) The binding energy of peak r as a function of the kinetic energy of photoelectrons. The green dashed lines indicate the uncertainty of ±0.18 cm^{-1}.

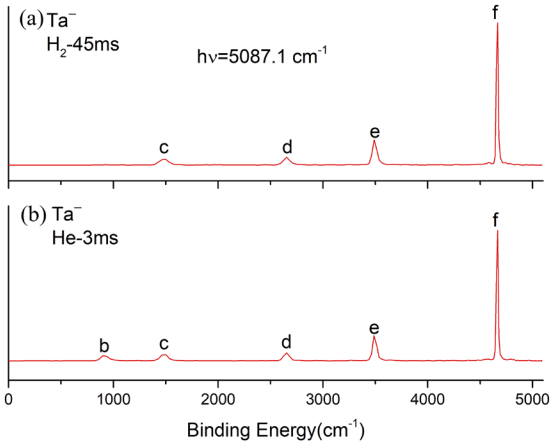

FIG. 3. Photoelectron energy spectra measured at photon energy $h\nu$ = 5087.1 cm^{-1} using a difference-frequency-generation laser. (a) Ta^- ions were trapped for 45 ms using H_2 as the buffer gas. (b) Ta^- ions were trapped for 3 ms using He as the buffer gas.

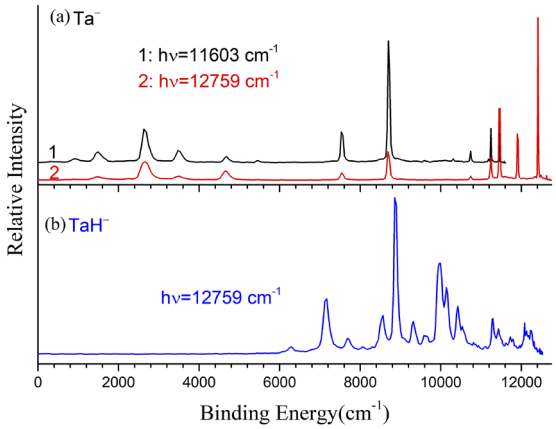

FIG. 4. Comparison of photoelectron energy spectra of Ta^- and TaH^-. (a) The spectra of Ta^- at photon energy $h\nu$ = 11 603 and 12 759 cm^{-1}. (b) The spectrum of TaH^- at $h\nu$ = 12 759 cm^{-1}.

Note that 1 eV = 8065.543 937 cm^{-1}, as recommended by 2018 CODATA (Committee on Data for Science and Technology).[41]

Multiple photodetachment channels from the excited states $^5D_1$ and $^5D_2$ of Ta^- were observed in the present work, which provided a cross-check for the assignment related to the two states. The energy level of $^5D_1$ can be determined accurately via the sharp peak o, and $^5D_2$ can be pinned down via peak k. However, only one broad peak *b* was assigned from the excited state $^3P_0$, which is different from the acquired spectrum at 488 nm by Feigerle *et al.*[19] They observed a few transitions from $^3P_0$. The possible reason for the difference is the different photon energy or any unknown contaminations. To determine the binding energy of peak b as accurately as possible, we collected the photoelectron energy spectra at a lower photon energy 5087.1 cm^{-1} using our DFG laser system. As shown in Fig. 3, peaks b–f became sharper compared to peaks in Fig. 1. Peak *a* could not be observed with the trap-on mode, which might be due to a relatively short lifetime of $^5D_2$. Interestingly, peak *b* disappeared when the buffer gas was changed from He to H_2, while peak *c* had no notable change. This means that the excited state $^3P_0$ can be effectively quenched via collisions with buffer gas H_2, but $^5D_1$ cannot be effectively quenched. To rule out the possible contamination of TaH^-, we also collected the

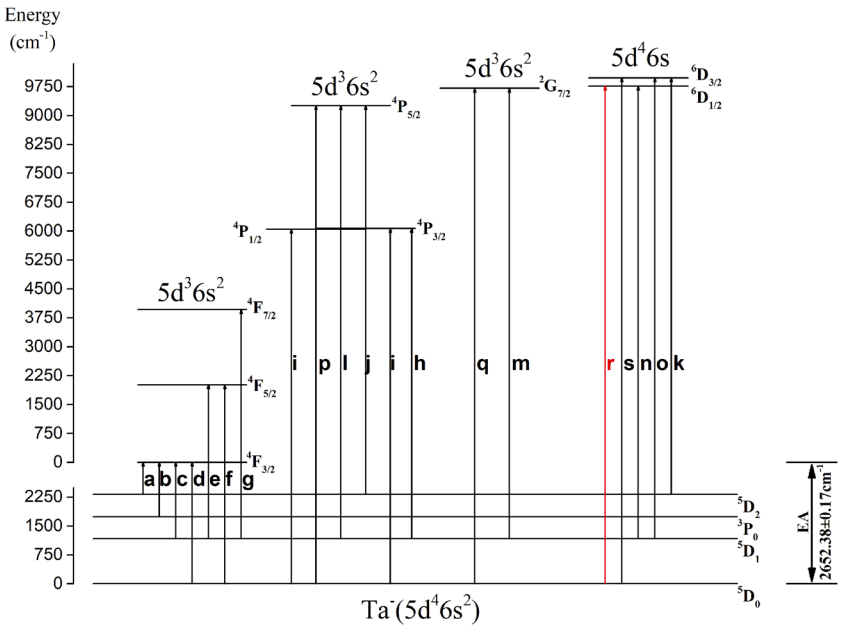

FIG. 5. Energy levels of Ta and Ta^- related to the present work. The ground state of Ta^- is $5d^46s^2\ ^5D_0$. The ground state of Ta is $5d^36s^2\ ^4F_{3/2}$. The labels of each transition are the same as the peaks observed in Figs. 1 and 3. Peak i is related to two transitions with a small gap 19.49 cm^{-1}, which cannot be resolved in the present work. Channel *r* marked in red is employed for the measurement of the electron affinity of Ta.

TABLE I. Measured binding energies and assigned binding energies of transitions observed in the present work.

Peak	Levels (Ta ← Ta$^-$)[a]	Measured binding energy (cm^{-1})	Assigned binding energy (cm^{-1})[b]
a	$(5d^36s^2)^4F_{3/2} \leftarrow {}^5D_2$	424(100)	332.3(20)
b	$(5d^36s^2)^4F_{3/2} \leftarrow {}^3P_0$	916.5(10)	916.5(10)
c	$(5d^36s^2)^4F_{3/2} \leftarrow {}^5D_1$	1 483.0(11)	1 482.74(17)
d	$(5d^36s^2)^4F_{3/2} \leftarrow {}^5D_0$	2 652.43(18)	2 652.38(17)
e	$(5d^36s^2)^4F_{5/2} \leftarrow {}^5D_1$	3 492.9(10)	3 492.87(17)
f	$(5d^36s^2)^4F_{5/2} \leftarrow {}^5D_0$	4 662.7(16)	4 662.51(17)
g	$(5d^36s^2)^4F_{7/2} \leftarrow {}^5D_1$	5 454(11)	5 446.66(17)
h	$(5d^36s^2)^4P_{3/2} \leftarrow {}^5D_1$	7 545(20)	7 551.70(17)
i	$(5d^36s^2)^4P_{3/2} \leftarrow {}^5D_0$ $(5d^36s^2)^4P_{1/2} \leftarrow {}^5D_0$	8 708(20)	8 701.81(17)/8 721.34(17)
j	$(5d^36s^2)^4P_{5/2} \leftarrow {}^5D_2$	9 606(40)	9 585.7(20)
k	$(5d^46s)^6D_{3/2} \leftarrow {}^5D_2$	10 308.0(20)	10 308.1(20)
l	$(5d^36s^2)^4P_{5/2} \leftarrow {}^5D_1$	10 735.5(10)	10 736.19(17)
m	$(5d^36s^2)^2G_{7/2} \leftarrow {}^5D_1$	11 186.2(18)	11 188.09(17)
n	$(5d^46s)^6D_{1/2} \leftarrow {}^5D_1$	11 242.27(50)	11 241.76(17)
o	$(5d^46s)^6D_{3/2} \leftarrow {}^5D_1$	11 458.54(19)	11 458.58(17)
p	$(5d^36s^2)^4P_{5/2} \leftarrow {}^5D_0$	11 906.2(10)	11 905.83(17)
q	$(5d^36s^2)^2G_{7/2} \leftarrow {}^5D_0$	12 338(40)	12 357.73(17)
r	$(5d^46s)^6D_{1/2} \leftarrow {}^5D_0$	12 411.40(18)	12 411.40(17)
s	$(5d^46s)^6D_{3/2} \leftarrow {}^5D_0$	12 628.06(61)	12 628.22(17)

[a]The electronic configuration of Ta$^-$ is $5d^46s^2$.
[b]Deduced value according to the assignment, the measured EA value, the optimized binding energy of transitions measured in the present work, and the energy levels of the neutral atom Ta.

photoelectron energy spectrum of TaH$^-$ at a temperature of 15 K using H_2 as the buffer gas. As shown in Fig. 4, there is no observable contamination from TaH$^-$ in our spectra of Ta$^-$. The interference from TaH$^-$ has been cleanly removed via the high-resolution mass spectrometer.

The assignment of all peaks observed in the present work was illustrated in Fig. 5 and was also listed in Table I. Since multiple transition energies were measured for each initial anionic state, a global optimization analysis based on covariance algebra was conducted to obtain the interval between any two energy levels.[42–45] Table II compared the energy levels of excited states of Ta$^-$ measured in the present work with that by Feigerle *et al.*[19] Table III summarizes the electron affinity of Ta in comparison with the previous results.

TABLE II. The energy levels of excited states of Ta$^-$ (cm^{-1}). The configuration of Ta$^-$ is $5d^46s^2$.

Levels	Feigerle *et al.*[19]	This work
${}^5D_1 \leftarrow {}^5D_0$	1070(110)	1169.64(17)
${}^3P_0 \leftarrow {}^5D_0$	1750(110)	1735.9(10)
${}^5D_2 \leftarrow {}^5D_0$	2240(120)	2320.1(20)

TABLE III. Electron affinity of Ta (eV).

EA	References
0.15	Zollweg[30] (calculated)
0.8(3)	Scheer[31] (measured)
1.0	Cole and Perdew[32] (calculated)
0.323(12)	Feigerle *et al.*[19] (measured)
0.31	Figgen *et al.*[33] (calculated)
0.328 859(23) or 2652.38(17) cm^{-1}	This work (measured)

In conclusion, the electron affinity of tantalum was measured to be 2652.38(17) or 0.328 859(23) eV. The accuracy has been improved by a factor of 500 with respect to the previous work. Moreover, the dense photodetachment channels of Ta anions were successfully resolved, and the energy levels of excited states of Ta anions were determined to be 1169.64(17) cm^{-1} ($^5D_1$), 1735.9(10) cm^{-1} ($^3P_0$), and 2320.1(20) cm^{-1} ($^5D_2$) above the ground state $^5D_0$, respectively. As demonstrated in the present work, the combination of a slow electron velocity-map imaging method and a cryogenic ion trap is a powerful tool that can be used to investigate other atomic and molecular species with complicated structures.[46]

ACKNOWLEDGMENTS

This work was s supported by the National Natural Science Foundation of China (NSFC) (Grant Nos. 11974199 and 91736102) and the National Key R&D Program of China (Grant No. 2018YFA0306504).

AUTHOR DECLARATIONS

Conflict of Interest

The authors have no conflicts to disclose.

Author Contributions

Sheng Li: Investigation (equal); Writing – original draft (equal). **Xiaoxi Fu:** Investigation (equal). **Xiaolin Chen:** Investigation (equal). **Yuzhu Lu:** Investigation (equal); Writing – review & editing (equal). **Chuangang Ning:** Conceptualization (equal); Investigation (equal); Writing – review & editing (equal).

DATA AVAILABILITY

The data that support the findings of this study are available from the corresponding author upon reasonable request.

REFERENCES

[1] R. C. Bilodeau and H. K. Haugen, Phys. Rev. Lett. **85**, 534 (2000).
[2] A. Kellerbauer and J. Walz, New J. Phys. **8**, 45 (2006).
[3] U. Warring, M. Amoretti, C. Canali, A. Fischer, R. Heyne, J. O. Meier, C. Morhard, and A. Kellerbauer, Phys. Rev. Lett. **102**, 043001 (2009).
[4] A. Fischer, C. Canali, U. Warring, A. Kellerbauer, and S. Fritzsche, Phys. Rev. Lett. **104**, 073004 (2010).

[5]L. Pan and D. R. Beck, Phys. Rev. A **82**, 014501 (2010).
[6]C. W. Walter, N. D. Gibson, D. J. Matyas, C. Crocker, K. A. Dungan, B. R. Matola, and J. Rohlén, Phys. Rev. Lett. **113**, 063001 (2014).
[7]E. Jordan, G. Cerchiari, S. Fritzsche, and A. Kellerbauer, Phys. Rev. Lett. **115**, 113001 (2015).
[8]G. Cerchiari, A. Kellerbauer, M. S. Safronova, U. I. Safronova, and P. Yzombard, Phys. Rev. Lett. **120**, 133205 (2018).
[9]Y. Z. Lu, R. L. Tang, X. X. Fu, and C. G. Ning, Phys. Rev. A **99**, 062507 (2019).
[10]C. W. Walter, N. D. Gibson, N. B. Lyman, and J. Wang, Phys. Rev. A **102**, 042812 (2020).
[11]M. S. Safronova, C. Cheung, M. G. Kozlov, S. E. Spielman, N. D. Gibson, and C. W. Walter, Phys. Rev. A **103**, 022819 (2021).
[12]C. W. Walter, N. D. Gibson, C. M. Janczak, K. A. Starr, A. P. Snedden, R. L. Field III, and P. Andersson, Phys. Rev. A **76**, 052702 (2007).
[13]C. W. Walter, N. D. Gibson, Y.-G. Li, D. J. Matyas, R. M. Alton, S. E. Lou, R. L. Field, D. Hanstorp, L. Pan, and D. R. Beck, Phys. Rev. A **84**, 032514 (2011).
[14]X.-X. Fu, R.-L. Tang, Y.-Z. Lu, and C.-G. Ning, Chin. Phys. B **29**, 073201 (2020).
[15]S. M. O'Malley and D. R. Beck, Phys. Rev. A **80**, 032514 (2009).
[16]R. Tang, R. Si, Z. Fei, X. Fu, Y. Lu, T. Brage, H. Liu, C. Chen, and C. Ning, Phys. Rev. Lett. **123**, 203002 (2019).
[17]R. Tang, R. Si, Z. Fei, X. Fu, Y. Lu, T. Brage, H. Liu, C. Chen, and C. Ning, Phys. Rev. A **103**, 042817 (2021).
[18]R. Tang, Y. Lu, H. Liu, and C. Ning, Phys. Rev. A **103**, L050801 (2021).
[19]C. S. Feigerle, R. R. Corderman, S. V. Bobashev, and W. C. Lineberger, J. Chem. Phys. **74**, 1580 (1981).
[20]X. Fu, Z. Luo, X. Chen, J. Li, and C. Ning, J. Chem. Phys. **145**, 164307 (2016).
[21]Z. H. Luo, X. L. Chen, J. M. Li, and C. G. Ning, Phys. Rev. A **93**, 020501(R) (2016).
[22]C. Hock, J. B. Kim, M. L. Weichman, T. I. Yacovitch, and D. M. Neumark, J. Chem. Phys. **137**, 244201 (2012).
[23]A. Osterwalder, M. J. Nee, J. Zhou, and D. M. Neumark, J. Chem. Phys. **121**, 6317 (2004).
[24]I. León, Z. Yang, H.-T. Liu, and L.-S. Wang, Rev. Sci. Instrum. **85**, 083106 (2014).
[25]R. Tang, X. Fu, and C. Ning, J. Chem. Phys. **149**, 134304 (2018).
[26]R. Tang, X. Fu, Y. Lu, and C. Ning, J. Chem. Phys. **152**, 114303 (2020).
[27]R. L. Tang, X. L. Chen, X. X. Fu, H. Wang, and C. G. Ning, Phys. Rev. A **98**, 020501(R) (2018).
[28]X. X. Fu, Y. Z. Lu, R. L. Tang, and C. G. Ning, Phys. Rev. A **101**, 022502 (2020).
[29]X. X. Fu, R. L. Tang, Y. Z. Lu, and C. G. Ning, Chin. J. Chem. Phys. **32**, 187 (2019).
[30]R. J. Zollweg, J. Chem. Phys. **50**, 4251 (1969).
[31]M. D. Scheer, J. Res. Natl. Bur. Stand., Sect. A **74A**(1), 37 (1970).
[32]L. A. Cole and J. P. Perdew, Phys. Rev. A **25**, 1265 (1982).
[33]D. Figgen, K. A. Peterson, M. Dolg, and H. Stoll, J. Chem. Phys. **130**, 164108 (2009).
[34]W. C. Wiley and I. H. McLaren, Rev. Sci. Instrum. **26**, 1150 (1955).
[35]B. Dick, Phys. Chem. Chem. Phys. **16**, 570 (2014).
[36]C. N. Yang, Phys. Rev. **74**, 764 (1948).
[37]J. Cooper and R. N. Zare, J. Chem. Phys. **48**, 942 (1968).
[38]J. Cooper and R. N. Zare, J. Chem. Phys. **49**, 4252 (1968).
[39]Y. Liu and C. Ning, J. Chem. Phys. **143**, 144310 (2015).
[40]A. Kramida, Y. Ralchenko, J. Reader, and NIST ASD Team, NIST Atomic Spectra Database (version 5.9), NIST, Gaithersburg, MD, https://physics.nist.gov/asd (retrieved 4 June, 2022).
[41]E. Tiesinga, P. J. Mohr, D. B. Newell, and B. N. Taylor, J. Phys. Chem. Ref. Data **50**, 033105 (2021).
[42]A. E. Kramida, Comput. Phys. Commun. **182**, 419–434 (2011).
[43]R. J. Peláez, C. Blondel, M. Vandevraye, C. Drag, and C. Delsart, J. Phys. B: At., Mol. Opt. Phys. **44**, 195009 (2011).
[44]X. Chen, Z. Luo, J. Li, and C. Ning, Sci. Rep. **6**, 24996 (2016).
[45]J. E. Sansonetti and W. C. Martin, J. Phys. Chem. Ref. Data **34**, 1559 (2005).
[46]C. Ning and Y. Lu, J. Phys. Chem. Ref. Data **51**, 021502 (2022).